JOURNAL OF SOLID STATE CHEMISTRY 16, 21–34 (1976)

The Electrical Conductivity and Thermodynamic Behavior of SrO-doped Nonstoichiometric Cerium Dioxide*

R. N. BLUMENTHAL AND J. E. GARNIER

Metallurgy and Materials Science, College of Engineering, Marquette University, Milwaukee, Wisconsin 53233

Received October 3, 1974; in revised form, April 23, 1975

Electrical conductivity and thermogravimetric measurements were made on SrO-doped nonstoichiometric cerium dioxide (i.e., $Ce_{1-y}Sr_yO_{2-y-x}$) as a function of temperature (~700–1500°C) and oxygen partial pressure (~1 to 10^{-21} atm). Assuming limiting case defect models the ionic, σ_i, and electronic, σ_e, conductivities were calculated from this data.

In the region where $y \gg x$ (i.e., at low temperatures and high oxygen pressures) the conductivity is independent of P_{O_2} and up to approximately 3 mole% SrO, it is proportional to mole% SrO. The equation for ionic conductivity, $\sigma_i \simeq [4.5 \pm 0.5]$[m/o SrO]$\exp(-0.58/kT)$, was obtained by fitting the conductivity data in this region to an expression derived on the basis of an oxygen vacancy model.

In the composition region between approximately $x = 10^{-3}$ and $x = 10^{-2}$, both the thermodynamic behavior and the electrical conductivity was shown to be consistent with a defect model involving randomly distributed doubly ionized oxygen vacancies and electrons localized on normal cerium sites. In this region the electronic conductivity varies linearly with x and the electronic mobility decreases with increasing SrO content.

Introduction

Although there have been several defect structure analyses based on the thermodynamic and/or electrical properties of "pure" nonstoichiometric oxides and doped-stoichiometric oxides, there have been very few of these types of analyses on doped-nonstoichiometric oxide systems. To help provide a better understanding of defect behavior in doped-nonstoichiometric oxide systems, we have initiated a comprehensive study in our laboratory to determine the effect of ionic radius, valence, and concentration of foreign cations on the thermodynamic and electrical behavior of doped-CeO_{2-x}. Cerium dioxide was selected as the host oxide in these doping experiments because it exhibits a large nonstoichiometric region (*1–5*) and an extensive solubility for foreign cations (*7*), and extensive studies have been performed on the thermodynamic (*2–6*) and electrical (*8–17*) behavior of "pure" CeO_{2-x}.

Based on studies of X-ray and neutron diffraction (*18*), thermodynamic (*4*, *5*), electrical conductivity (*16*, *17*), and oxygen diffusion (*19*), the predominant defects in nonstoichiometric CeO_2 are doubly ionized oxygen vacancies and electrons localized on normal cerium atoms.

The doping experiments on CeO_{2-x} were initiated using CaO because the calcium ion has an ionic radius similar to a cerium ion and the addition of CaO to CeO_2 results in the formation of oxygen vacancies (*20*). Thus, the solution of CaO in nonstoichiometric cerium dioxide may be represented by the formula $Ce_{1-y}Ca_yO_{2-y-x}$. The results of a recent study (*20*) in this laboratory on the electrical

* Supported by the U.S. Atomic Energy Commission, Division of Research. This is AEC Report COO-1441-25.

conductivity of CaO-doped (0.1 to 16 mole%) cerium dioxide as a function of P_{O_2} (i.e., 1 to 10^{-22} atm) and temperature (i.e., 700 to 1500°C) have been reported (*20*).

Two limiting case conductivity regions were observed in that study (*20*). At low temperatures and high oxygen pressures, the conductivity is predominantly ionic. In this region, the conductivity is independent of P_{O_2} and between approximately 1 and 8 m/o CaO is proportional to mole% CaO. The following equation for ionic conductivity

$$\sigma_i \simeq [6.0 \pm 0.5][\text{m/o CaO}]\exp^{-0.62/kT} \quad (1)$$

was obtained by fitting the conductivity data in this region to an expression derived on the basis of an oxygen vacancy model. At high temperatures and low oxygen partial pressures and for lower CaO content the conductivity is predominantly electronic.

A thermogravimetric study on CaO-doped nonstoichiometric cerium dioxide (i.e., $Ce_{1-y}Ca_yO_{2-y-x}$) in the temperature range 800–1500°C and from oxygen pressures of 10^{-1} to 10^{-21} atm has been reported recently (*21*). From these data the deviation from stoichiometry $x = x(T,P_{O_2})_y$ was determined for values of $y = 0.01$, 0.045, 0.07, 0.10, and 0.14. The thermodynamic quantities $\Delta\bar{H}_{O_2}$ and $\Delta\bar{S}_{O_2}$ were calculated in the region $0.001 \leqslant x \leqslant 0.2$ and they were found to be independent of temperature with the exception of the 14 mole % CaO at large deviations from stoichiometry.

In the composition region near stoichiometry (i.e., for x between approximately 10^{-3} and 10^{-2}), the variation of $\Delta\bar{S}_{O_2}$ with x was consistent with a defect model involving randomly distributed doubly ionized oxygen vacancies and electrons localized on normal cerium sites. The experimental observation that $x \propto P_{O_2}{}^{-1/4}$ was rationalized on the basis of the above defect model for the case where $y > x$.

At large deviations from stoichiometry, the dependence of $x = x(T,P_{O_2})_y$ is similar to the nonstoichiometric behavior of pure CeO_{2-x} when $y = 0.01$ or 0.045. The dependence of $\Delta\bar{H}_{O_2}$ and $\Delta\bar{S}_{O_2}$ on x is also similar. However, for $y = 0.07$, 0.10, and 0.14, the nonstoichiometric behavior and the dependence of $\Delta\bar{H}_{O_2}$ on x differs significantly from the behavior of pure CeO_{2-x}.

In the above studies, CaO was selected as a dopant because the ionic radius of the calcium ion (Ca^{2+}:1.09 Å) is very similar to the cerium ion (Ce^{4+}:1.07 Å) (*7*). In the current study, SrO was selected as a dopant to determine the effect of a larger cation (Sr^{2+}:1.14 Å) (*7*) with the same valence as Ca^{2+} on the thermodynamic and electrical behavior of doped nonstoichiometric cerium dioxide.

Theory

A. Defects Formed by Doping CeO_2 with SrO

It is generally assumed that doping CeO_2 with SrO produces oxygen vacancies. To test the oxygen vacancy model, a room temperature study was made in this laboratory comparing the true density and calculated values of the density based on lattice parameter data. The true density was determined using a water pycnometric technique. The measurements were made on powder obtained by crushing and grinding the sintered SrO-doped CeO_2 specimens in an alumina mortar and pestle. With this procedure, the problem associated with porosity in the powder was eliminated. The results of this study, for specimens in the stoichiometric condition with SrO contents between 0.1 and 10 m/o, are shown in Fig. 1. Curves A and B, corresponding to Eqs. (2) and (3), respectively,

$$\text{SrO} \rightarrow \text{Sr}_i^{\cdot} + \text{O}_i'' \quad (2)$$

$$\text{SrO} \rightarrow \text{Sr}_i^{\cdot} + \tfrac{1}{2}V_{Ce}'''' + \text{O}^x{}_o, \quad (3)$$

were calculated assuming strontium ions occupy cerium interstitial sites and the formulation of charge-compensating defects which can be oxygen interstitial or cerium vacancies. (The notation used to identify defects in this paper is the same as used by Kröger (*22*).) Curves B and C, corresponding to Eqs. (4) and (5), respectively,

$$\tfrac{1}{2}\text{Ce}^x_{Ce} + \text{SrO} \rightarrow \text{Sr}''_{Ce} + \tfrac{1}{2}\text{Ce}_i'''' + \text{O}^x{}_o \quad (4)$$

$$\text{SrO} \rightarrow \text{Sr}''_{Ce} + V_o^{\cdot\cdot} + \text{O}^x{}_o, \quad (5)$$

were calculated assuming strontium ions occupy cerium sites and the formation of charge-compensating defects which can be

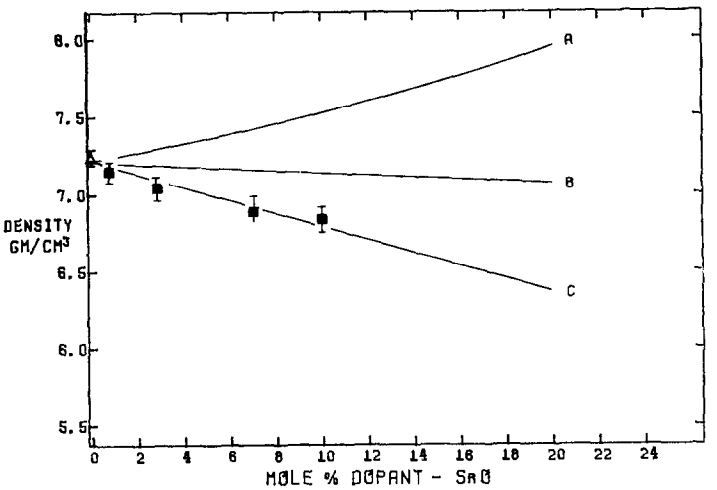

FIG. 1. Comparison of pycnometric density and calculated values of the density based on lattice parameter data for specimens of CeO_2 doped with SrO between 1 and 7 mole%.

cerium interstitial or oxygen vacancies. The lattice parameter data used in these calculations is shown in Fig. 2.[1] It is interesting to note that the results of the lattice parameter study appear to be in agreement with experimental error with the reported solubility (*7*) of SrO in CeO_2 (i.e., 9 mole% SrO in air at 1600°C). Unfortunately, the effect of temperature and oxygen pressure on the solubility limits is not known. The data points shown in Fig. 1 correspond to the room temperature true density measurements. The agreement between the experimental data and curve C confirms the existence of oxygen vacancies in $Ce_{1-y}Sr_yO_{2-y}$.

B. Nonstoichiometric Defect Model for SrO-Doped Cerium Dioxide

As discussed above, the results of recent thermodynamic studies (*4*, *5*, *21*) on CeO_{2-x} and $Ce_{1-y}Ca_yO_{2-y-x}$ employing a thermogravimetric technique to determine $x = x(P_{O_2}, T)_y$ are consistent with a predominant nonstoichiometric defect model involving doubly ionized oxygen vacancies, $V_o^{\cdot\cdot}$, and electrons localized on normal cerium atoms, Ce'_{Ce}.

If the same nonstoichiometric defect reaction for CeO_{2-x} and $Ce_{1-y}Ca_yO_{2-y-x}$

$$2Ce^x_{Ce} + O^x_o = \tfrac{1}{2}O_2(g) + V_o^{\cdot\cdot} + 2Ce'_{Ce} \quad (6)$$

is assumed to occur in $Ce_{1-y}Sr_yO_{2-y-x}$, then the entropy change for the defect reaction in Eq. (6) may be expressed by

$$\Delta S = \bar{S}_{V_o^{\cdot\cdot}} + 2\bar{S}_{Ce'_{Ce}} + \tfrac{1}{2}S^o_{O_2} - 2\bar{S}_{Ce^x_{Ce}} - S^x_{O_o}, \quad (7)$$

where the oxygen gas is taken to be at 1 atm and the relative partial molal entropy, $\Delta\bar{S}_{O_2} = -2\Delta S$. The quantity $S^o_{O_2}$ is approximately equal to 60 entropy units in the temperature range of this investigation. The partial molal terms, $\bar{S}_i$, may be divided into vibrational, S_i^v, and configurational, S_i^c, terms. If the defects are randomly distributed

$$S_i^c = -R \ln x_i, \quad (9)$$

where x_i is the site fraction of species i. For this case it can readily be shown that

$$-\Delta\bar{S}_{O_2} = 2\Delta S = S^o_{O_2} + 2S^v_t - 2R \ln\left[\frac{x+y}{2}\right] - 4R \ln[2x] + 4R \ln[1-y-2x] + 2R \ln\left[1 - \frac{x+y}{2}\right], \quad (10)$$

[1] See NAPS document No. 02619 for 7 pages of supplementary material. Order from ASIS/NAPS c/o Microfiche Publications, 440 Park Avenue South, New York, N.Y. 10016. Remit payment in advance for each NAPS accession number. Make checks payable to Microfiche Publications. Photocopies are $5.00. Microfiche are $1.50. Outside of the United States and Canada, postage is $2.00 for a photocopy or $0.50. for a fiche. Figs. 2, 7, 9, 11, and 13 are deposited with NAPS; they are not included herein.

where ΔS_t^v is the total vibrational entropy change (*21*). If a first-order approximation is made, that is, the vibrational terms are assumed independent of x and y, then the compositional dependence of $\Delta \bar{S}_{O_2}$ may be expressed by Eq. (10) as a function of x and y.

C. Defect Model for Ionic Conductivity

The simplest model for ionic conduction in SrO-doped CeO_2 is to assume that the ionic conduction occurs by the migration of oxygen vacancies with only one state of ionization, $V_o^{\cdot\cdot}$. For this case the ionic conductivity, σ_i, may be represented by the expression

$$\sigma_i = 2B[V_o^{\cdot\cdot}]e\mu_{V_o^{\cdot\cdot}}, \qquad (11)$$

where the bracketed term represents the number of a given species divided by the number of sites available for that species, B is a parameter that relates the concentration in site fraction to number per cubic centimeter, e is the charge on an electron, and $\mu_{V_o^{\cdot\cdot}}$ is the mobility of doubly ionized oxygen vacancies. If the oxygen vacancies are isolated point defects randomly distributed and the concentration of nonstoichiometric defects is small (i.e., $y > x$), then

$$[V_o^{\cdot\cdot}] = (\text{m/o SrO})/200 \qquad (12)$$

In addition, if $\mu_{V_o^{\cdot\cdot}}$ is assumed to be a function of temperature only, then

$$\mu_{V_o^{\cdot\cdot}} = \mu'_{V_o^{\cdot\cdot}} \exp(-E_i/kT). \qquad (13)$$

Combining Eqs. (11), (12), and (13), the relation for ionic conductivity is

$$\sigma_i = A(\text{m/o SrO}) \exp(-E_i/kT), \qquad (14)$$

where

$$A = B\mu'_{V_o^{\cdot\cdot}} e/100. \qquad (15)$$

Equation (8) may be tested in a region near stoichiometry, where the ionic conduction predominates (i.e., $\sigma \simeq \sigma_i$) by observing if σ is directly proportional to the SrO content in this region. In the region of this limiting case, σ also should be independent of P_{O_2}.

D. Models for Electronic Conduction

In a recent study, the isothermal compositional dependence of the electrical conductivity of CeO_{2-x} was determined by combining thermodynamic data, $x = x(P_{O_2},T)$, with the appropriate electrical conductivity data, $\sigma = \sigma(P_{O_2},T)$ (*17*). The compositional dependence of the electrical conductivity of CeO_{2-x} was represented by the expression

$$\sigma = 410\ [x]e^{-(0.158+x)/kT}\ (\text{ohm-cm})^{-1} \qquad (16)$$

over the temperature range 750 to 1500°C and from $x = 0.001$ to $x = 0.1$.

Equation (16) was rationalized in terms of the following simple relations for (a) the electron carrier concentration

$$n_{Ce'_{Ce}} = 8x/a_o^3 \qquad (17)$$

where $n_{Ce'_{Ce}}$ is the number of Ce'_{Ce} per cubic centimeter and a_o is the lattice parameter, and (b) the electron mobility

$$\mu_e = 5.2(10^{-2})e^{-(0.158+x)/kT}\ (\text{cm}^2/\text{V-sec}). \qquad (18)$$

Assuming the nonstoichiometric defect reaction in $Ce_{1-y}Sr_yO_{2-y-x}$ is given by Eqs. (6) and (17) is valid, then the electronic conductivity may be represented by either of the following expressions

$$\sigma_e = n_{Ce'_{Ce}} e\mu_e \qquad (19)$$

or

$$\sigma_e = \frac{8}{a_0^3}[x]e\mu_e. \qquad (20)$$

Although it should be possible to represent the electronic mobility in $Ce_{1-y}Sr_yO_{2-y-x}$ by an expression of the type

$$\mu_e = \mu_o\, e^{-Q/kT}, \qquad (21)$$

the values for μ_o and Q would not be the same as given in Eq. (18) for pure CeO_{2-x} because of the presence of SrO. However, for small deviations from stoichiometry (e.g., $10^{-3} x < 10^{-2}$), μ_e should be relatively insensitive to x and we would expect that for isothermal conditions in this composition region (*17*)

$$\sigma_e \alpha x. \qquad (22)$$

Experimental

A. Sample Preparation

Conductivity and thermodynamic specimens of CeO_2 doped with SrO (0.1–7.0 m/o SrO) were prepared by dry-mixing the appropriate proportions of CeO_2 and SrO powder. The results of a mass spectrographic

analysis on the CeO_2 powder are given in a previous publication (*20*). These powders were then pressed into bars $2 \times \frac{1}{4} \times \frac{1}{4}$ in. with a pressure of 20,000 psi. The bars were placed in an alumina boat and completely covered with SrO-doped CeO_2 powder of the same composition to minimize contamination of the specimen and to avoid loss of SrO during sintering. A molybdenum wound resistance furnace was used to sinter the bars at 1650°C for 3 hr in an argon atmosphere. Conductivity specimens were cut from the sintered bars to an average length of 2 cm and the thermodynamic specimens were cut into the shape of parallelpipeds weighing approximately 0.5 g. The bulk density measurements were determined from the mass of the specimen and the volume, which was obtained from the external dimensions of the specimen.

B. Thermodynamic Measurements

The experimental objective of the thermodynamic study was to determine the equilibrium deviation from stoichiometry, x, in SrO-doped cerium dioxide samples (i.e., $Ce_{1-y}Sr_yO_{2-y-x}$) as a function of temperature and oxygen partial pressure for values of y equal to 0.01 and 0.07. A thermogravimetric technique employing a Cahn R. G. microbalance was used to measure the changes in weight experienced by samples of SrO-doped CeO_2 as the external variables of temperatures and oxygen partial pressures were changed relative to a thermodynamic reference state of $(T, P_{O_2} = 0.1 \text{ atm})_y$ (*21, 22*). It was particularly important that the determination of the individual weight changes occurred over the shortest possible time periods, thus avoiding errors due to balance drift and local disturbances. Since the oxidation rates of CeO_2 are extremely high, the relative weight measurements were made from the reduced to the oxidized state. No evidence of compositional hysteresis was observed when these measurements were compared with those made from oxidized to reduced states. The experimental apparatus and procedure employed was the same as that described in previous studies (*4, 5, 21, 23*).

Temperatures from 800–1500°C were obtained with a molybdenum wound resistance furnace, measured with a reference grade Pt–Pt/13% Rh thermocouple and controlled to approximately $\pm\frac{1}{2}$°C with a Barber–Coleman model 477 capacitrol and a model 621 power controller. Controlled oxygen partial pressures for 10^{-1} to 10^{-21} atm were obtained from premixed and analyzed O_2–Ar and CO–CO_2 mixtures. Linear gas velocities ranged from 2.5 to 4.0 cm/sec, which is greater than the 0.9 cm/sec value recommended by Darken and Gurry (*24*) to eliminate thermal separation effects.

C. Electrical Conductivity Measurements

The electrical conductivity measurements on SrO-doped cerium dioxide specimens as a function of P_{O_2} in the temperature range 700–1500°C were made in a molybdenum wound resistance furnace. A standard four-probe dc technique was employed for the electrical conductivity measurements. The experimental apparatus employed was essentially the same as that described in earlier publications (*13, 20*).

Controlled oxygen partial pressures for 10^{-1} to 10^{-21} atm were obtained from premixed and analyzed O_2–Ar and CO–CO_2 mixtures. A linear flow rate of 0.9 cm/sec was maintained for all gas mixtures used in this investigation to avoid errors arising from thermal diffusion (*24*). Electrical conductivity measurements were made at 100°C temperature intervals between 700 and 1500°C for a fixed gas mixture for both increasing and decreasing temperature, and at various gas mixtures for a fixed temperature for both increasing and decreasing P_{O_2}. Since the nonstoichiometric composition of SrO-doped ceria has a unique value for each SrO content, oxygen partial pressure, and temperature, the above technique ensured the measurement of equilibrium conductivity because the nonstoichiometric equilibrium state was approached from both higher and lower compositions of oxygen.

Results and Discussion

A. Thermodynamic Study

Thermogravimetric measurements were made on SrO-doped nonstoichiometric cerium

dioxide specimens (1 and 7 mole% SrO) as a function of temperature (800–1500°C) and oxygen pressure (0.1 to 10^{-21} atm).

The deviation from stoichiometry calculated from the thermogravimetric measurements employing the procedure described in previous publications (*4*, *5*, *23*, *24*) is shown in Fig. 3, where isotherms of log x in $Ce_{1-y}Sr_yO_{2-y-x}$ are plotted versus log P_{O_2} for $y = 0.01$ and 0.07, respectively. Although isothermal values of x for the sample doped with 1% SrO were obtained in 25°C increments between 800–1050°C and 100°C intervals between 1100 and 1500°C, only the results at 100°C intervals between 800 and 1500°C are shown to simplify the presentation of the results. For the sample doped with 7 mole% SrO, the data are limited to isotherms above 1000°C because of experimental problems observed below this temperature. Below 1000°C, the reduced sample gained weight very rapidly when the reference state atmosphere of $P_{O_2} = 0.1$ atm was introduced into the measuring system. After the rapid initial weight gain an additional weight gain was observed to occur at a much slower rate. The magnitude of this "second" weight gain decreased with increasing temperature until at 1000°C it was no longer observable. It should be noted that the "second weight gain" was not observed for pure (*4*, *5*), CaO-doped (*21*, *23*), and 1 mole% SrO-doped CeO_2 samples. Although on the basis of the results available at this time it is difficult to explain this behavior, it is possible that it may be related to decreasing solubility of SrO with decreasing temperature. The region to the right of the dashed line in this figure represents the region where the error in x is less than ±2%. The error bars for small deviation from stoichiometry are illustrated in the lower right-hand corner of Fig. 3. The precision for large deviations from stoichiometry was found to be ±0.2 to 0.3% (*4*) and may be adequately represented by the size of the data points. For comparative purposes x in pure CeO_{2-x} is shown as a solid line in this figure (*4*, *5*).

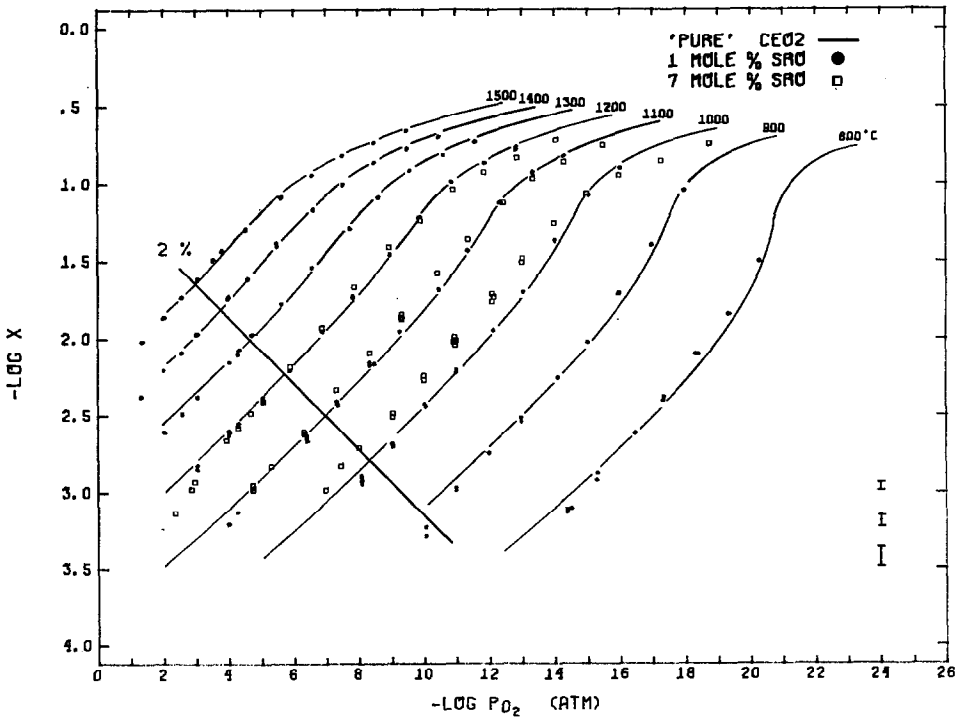

FIG. 3. A comparison of the isothermal plot of log x versus log P_{O_2} for SrO-doped CeO_2 (1 and 7 mole%) and pure nonstoichiometric CeO_2.

At small deviations from stoichiometry (i.e., for x less than approximately 0.01) the data is best characterized by the relation

$$x \propto P_{O_2}^{-1/4}. \tag{23}$$

Increasing the SrO content increases the range of nonstoichiometry for which Eq. (23) applies. It is interesting to note that this behavior was also observed for CaO-doped CeO_2 (*21*).

The relative partial molal enthalpy, $\Delta\bar{H}_{O_2}$, and entropy, $\Delta\bar{S}_{O_2}$, of oxygen were calculated from a least-squares fit of log P_{O_2} versus $1/T$, where $\Delta\bar{H}_{O_2}$ is proportional to the slope,

$$\Delta\bar{H}_{O_2} = R\left[\frac{\partial \ln P_{O_2}}{\partial 1/T}\right]_{x,y} \tag{24}$$

and $\Delta\bar{S}_{O_2}$ is proportional to the intercept at $1/T = 0$.

The calculations of $\Delta\bar{H}_{O_2}$ and $\Delta\bar{S}_{O_2}$ were restricted to temperatures and P_{O_2}'s where the errors in the x were less than 2%. Both $\Delta\bar{H}_{O_2}$ and $\Delta\bar{S}_{O_2}$ were found to be independent of temperature for the 1 mole% SrO sample. Because of the limited number of isotherms available no attempt was made to calculate $\Delta\bar{H}_{O_2}$ or $\Delta\bar{S}_{O_2}$ for the 7 mole% SrO-doped CeO_2 specimen.

$\Delta\bar{H}_{O_2}$ is plotted versus log x in Fig. 4 for the 1% SrO specimen. The error bars shown for different values of x are based on 95% confidence levels. For comparative purposes the results of a recent study (*4*, *5*) on pure CeO_{2-x} are also represented in Fig. 4. Discussion of the dependence of $\Delta\bar{H}_{O_2}$ on x are directed toward two different regions of x.

In the composition region near stoichiometry (i.e., for approximately $10^{-3} < x < 10^{-2}$) $\Delta\bar{H}_{O_2}$ exhibits only a slight dependence on x. It is interesting to note that in this composition range the value of $\Delta\bar{H}_{O_2}$ is larger for the 1 mole% SrO than for pure CeO_{2-x}.

At large deviations from stoichiometry, the dependence of $\Delta\bar{H}_{O_2}$ on x for the 1 mole% SrO appears to be similar to that observed for pure CeO_{2-x}.

The dependence of $\Delta\bar{S}_{O_2}$ on x is shown in Fig. 5, where $\Delta\bar{S}_{C_2}$ is plotted versus log x for the 1 mole% SrO specimen. Discussion of the dependence of $\Delta\bar{S}_{O_2}$ on x is directed towards two different regions of x.

To test the proposed defect model for the dependence of $\Delta\bar{S}_{O_2}$ on x, Eq. (10) was used to calculate $\Delta\bar{S}_{O_2}$ as a function of x for $y = 0.01$. In this calculation the quantity ΔS_t^v was arbitrarily taken as zero (*4*, *5*, *21*, *23*). The results of these calculations are shown by the solid line in Fig. 5. In the region near

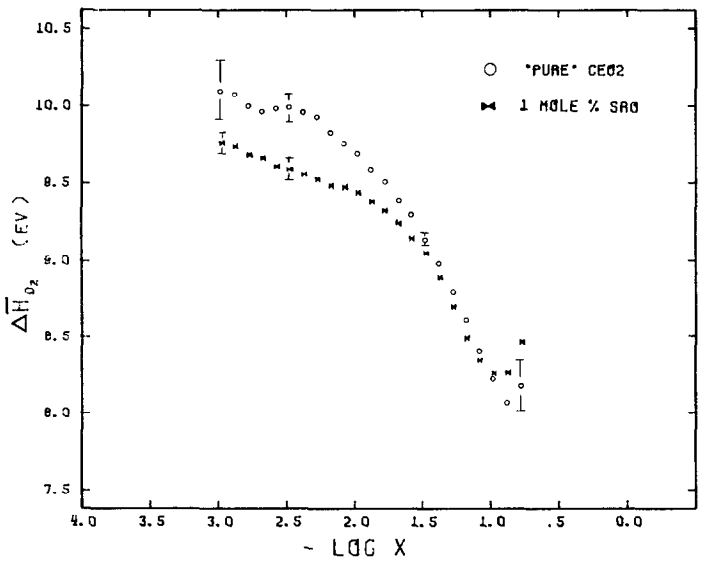

FIG. 4. A comparison plot of $\Delta\bar{H}_{O_2}$ versus log x for pure and 1 mole% SrO-doped CeO_2.

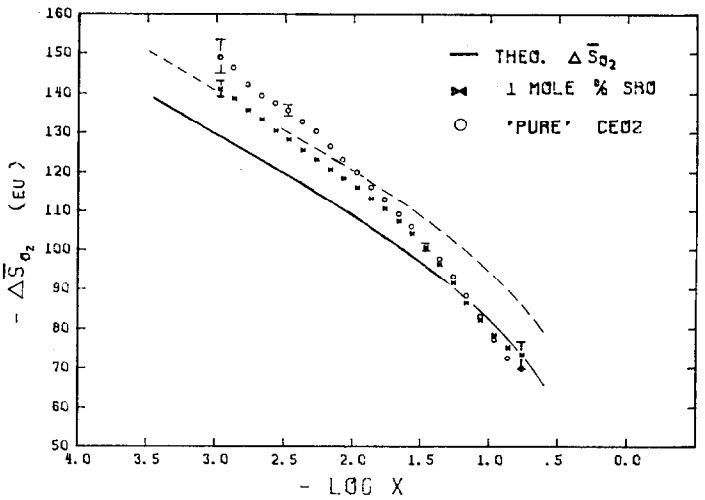

FIG. 5. A comparison plot of calculated (Eq. (10)) and measured values of $\Delta\bar{S}_{O_2}$ versus log x for 1 mole% SrO-doped CeO_2.

stoichiometry, the agreement between the calculated values and the measured values are quite good considering the assumption that ΔS_t^v is small and independent of x. The most striking observation, however, is the good agreement between the slope of the $\Delta\bar{S}_{O_2}$ versus log x curve calculated from Eq. (10), which is represented by the dashed line in Fig. 5 and the experimentally determined value. Thus, in this composition region, it appears that ΔS_{O_2} is consistent with a random distribution of doubly ionized oxygen vacancies and electrons localized on normal cerium atoms. It can be readily shown using the law of mass action that the observed dependence of $x \propto P_{O_2}^{-1/4}$ is also consistent with this defect model in the region where $\Delta\bar{H}_{O_2}$ is independent on x and $y > x$ (*23*).

At large deviations from stoichiometry, the calculated dependence of $\Delta\bar{S}_{O_2}$ on x deviates from the measured dependence of $\Delta\bar{S}_{O_2}$. This is the same region where $\Delta\bar{H}_{O_2}$ exhibits a significant dependence on x. This behavior is probably due to an increase in the defect–host interaction and undoubtedly the onset of defect–defect interaction.

B. Electrical Conductivity Study

The electrical conductivity of sintered specimens of strontia-doped nonstoichiometric cerium dioxide (0.1, 1.0, 3.0, and 7.0 mole% SrO) was measured as a function of temperature (i.e., 700 to 1500°C) and oxygen pressure (1 to 10^{-21} atm). Typical behavior of the conductivity as a function of the reciprocal absolute temperature in Ar–O_2 and CO–CO_2 mixtures is illustrated in Fig. 6 for a nonstoichiometric cerium dioxide specimen doped with 1.0 mole% SrO. The measured values of the conductivity, σ_{meas}, for the sintered specimen have been corrected for porosity using the relation (*15*):

$$\sigma = \sigma_{meas}(\rho_{theor}/\rho_{meas}), \qquad (25)$$

where ρ_{theor} is the theoretical density and ρ_{meas} is the bulk density of the sintered specimen. For all of the SrO-doped specimens two distinct types of behavior are observed in Fig. 6. At lower temperatures and high oxygen pressures (i.e., Ar–O_2 mixtures), the conductivity is independent of oxygen partial pressure and exponentially dependent on temperature. At higher temperatures and low oxygen pressures, the conductivity exhibits n-type behavior. Based on the simple limiting case defect model discussed in the theory section, the ionic conductivity should be proportional to mole% SrO and independent of P_{O_2} in the region near stoichiometry where $y > x$. Isothermal plots of log σ versus log P_{O_2} were made for each of the SrO-doped specimens to test this simple defect model.

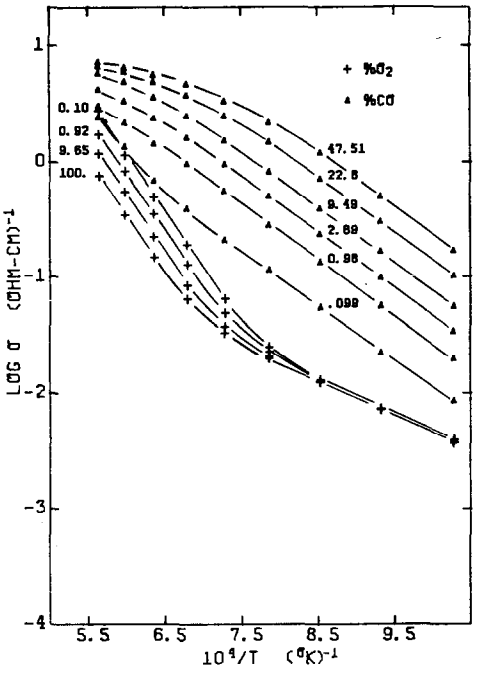

FIG. 6. Log σ versus $1/T$ for 1 mole% SrO-doped CeO_2 in Ar–O_2 and CO–CO_2 mixtures.

Typical plots are shown in Figs. 7, 8, and 9 for 1, 3, and 7 mole% SrO, respectively. For comparative purposes, the conductivity (*13*) of a pure CeO_2 specimen is shown as a dashed line in these figures.

A qualitative explanation of the observed electrical conductivity data may be given in terms of three regions as follows.

Region I. At low temperatures and high oxygen partial pressures (i.e., near stoichiometric conditions), the conductivity of the SrO-doped specimen is independent of oxygen partial pressure. The σ is also much larger than that of pure CeO_2. Since σ_i is to a first-order approximation independent of the oxygen pressure, this observation is consistent with a conduction process which is primarily ionic (i.e., $\sigma \simeq \sigma_i > \sigma_e$).

Region II. At high temperatures and particularly at low oxygen pressures, the σ of the SrO-doped specimens exhibits a similar P_{O_2} dependence as pure CeO_2. The conductivity in this region appears to be predominantly electronic (i.e., $\sigma \simeq \sigma_e > \sigma_i$) and is probably controlled by the same nonstoichiometric

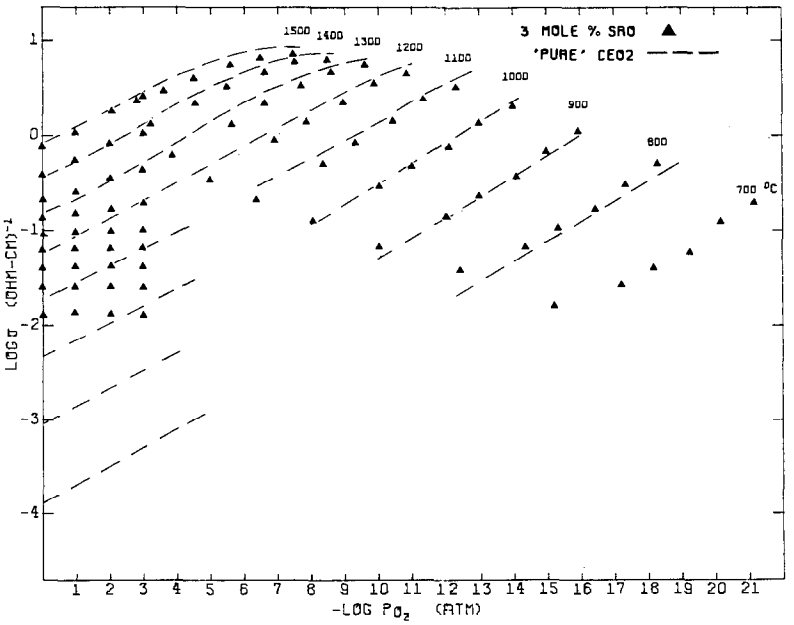

FIG. 8. A comparison of the isothermal plot of log σ versus log P_{O_2} for pure nonstoichiometric cerium dioxide and 3.0 SrO-doped CeO_2 sintered specimen.

defects as in pure CeO_2. As the SrO content increases, lower oxygen pressures (i.e., a higher concentration of nonstoichiometric defects) are required to "mask" out the effect of the SrO.

Region III. For all oxygen pressures and temperatures intermediate to Regions I and II, the conductivity appears to be mixed, i.e., where σ_e and σ_i are of the same order of magnitude.

According to Eq. (14), σ_i is proportional to the SrO content when $y > x$. To illustrate the effect of the SrO dopant concentration on σ, isothermal plots were made of log σ versus log mole% SrO for all of the gas mixtures used in this study. Typical plots of log σ versus log mole% SrO are shown in Figs. 10 and 11 for atmospheres containing 100% O_2 and 47.5% CO, respectively. The same three regions of behavior discussed above may be observed. In Region I (i.e., $\sigma \simeq \sigma_i$), the slope of log σ versus log % SrO is approximately one. This region is observed primarily at lower temperatures and higher oxygen pressures. For example, in an atmosphere of 100% O_2 (Fig. 10), this region extends from approximately 0.1 to 3 mole% SrO at 700°C. As the temperature increases from 700°C the lower limit for the SrO compositions, where σ_i is approximately proportional to mole% SrO increases. This occurs because of an increase in the electronic conduction (Eq. (20)), which is a result of an increase in the deviation from stoichiometry, x, with increasing temperature. In Region II (i.e., $\sigma \simeq \sigma_e$), the conductivity is almost independent of SrO content. This region extends to higher SrO compositions and lower temperatures in more reducing gas mixtures (i.e., lower oxygen partial pressures, see Fig. 11). Region III is a region of mixed conduction. Another interesting observation from Fig. 10 is that at high SrO compositions and lower temperatures, where σ_i predominates, the conductivity appears to exhibit a maximum with increasing SrO content. Similar behavior has been reported for CaO-doped CeO_2 and other fluorite oxide systems doped with lower valent cations. Two different models have been used to explain the maximum in σ observed in CaO-doped ZrO_2 (*24*). One model is based on a clustering of defects and the other on synthetic zones of composition. In both of these models, the activation energy increases with increasing CaO content. In contrast to the predictions of these models, the activation energy for both SrO and CaO-doped CeO_2 (*20*) determined from plots of log σ versus $1/T$ at 1 atm of O_2 appears to be independent of dopant content. It should be noted that the apparent maximum in σ occurs at a lower dopant concentration (~7 mole%) of SrO than for CaO (~10mole%) (*20*). Although the reported solubility (*7*) is 9 mole% SrO in air at 1600°C, the dependence of temperature and oxygen pressure on the solubility limits of SrO-doped CeO_2 is not known. Thus, the question of whether the concentration of SrO in this region exceeds the solubility of SrO in CeO_2 cannot be ascertained easily. Since the apparent maximum in σ occurs at a lower dopant concentration for SrO and the solubility of SrO is less than CaO, it appears that the concentration where the maximum in σ occurs may be related to the solubility limit of the dopant.

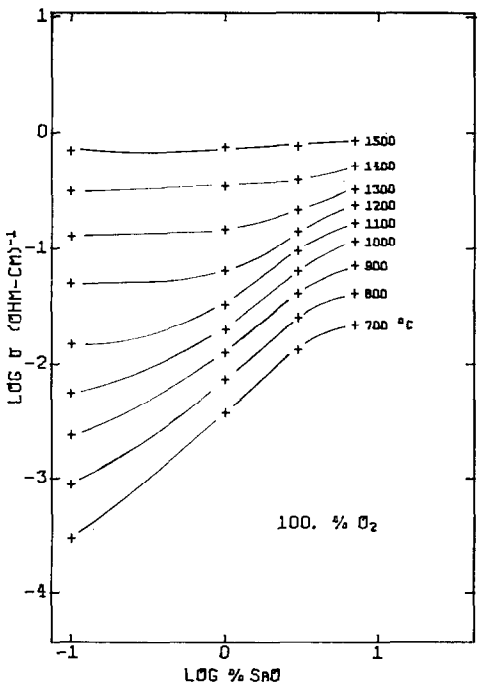

FIG. 10. Isothermal plot of log σ versus log mole% SrO in CeO_2 in 100% O_2.

The qualitative interpretation of the electrical behavior of SrO-doped CeO_2 observed in this study may be summarized as follows. SrO-doped CeO_2 exhibits both electronic and ionic conductivity. Two limiting case regions were observed. At low temperatures and high oxygen pressures, and SrO contents between approximately 0.1 and 3 mole% SrO, the conductivity is proportional to mole% SrO and is predominantly ionic, whereas at high temperatures and low oxygen partial pressures and lower SrO contents the conductivity is predominantly electronic.

In order to quantitatively analyze the proposed oxygen vacancy model for ionic conductivity, Eq. (14), the conductivity in the region where ionic conductivity predominated was plotted as a function of SrO. These results are shown in Fig. 12 at $P_{O_2} = 1$ atm for 700–1000°C and for SrO contents between 1 and 7 mole%. A direct proportionality was observed for specimens with SrO contents between approximately 1 and 3 mole% SrO. The parameter E_i in Eq. (14) was obtained from the plot shown in Fig. 13 of $\log \sigma$ versus $1/T$ at $P_{O_2} = 1$ atm for several different SrO contents. The average value of E_i determined from a least-squares analysis was 0.58 ± 0.03 eV for compositions from 1.0 to 7.0 mole% SrO. A value of $A = 4.5 \pm 0.5$ was determined by curve-fitting Eq. (14) to the data shown in Fig. 13. Thus, if the proposed limiting case defect model for ionic conductivity is correct the ionic conductivity in the composition region below 3 mole% SrO may be approximated by the relation

$$\sigma_i \simeq 4.5 \pm 0.5[\text{mole\% SrO}]\exp - (0.58/kT). \quad (26)$$

An approximation expression for the diffusion coefficient of oxygen vacancies, $D_{V_O^{\cdot\cdot}}$, in SrO-doped CeO_2

$$D_{V_O^{\cdot\cdot}} \simeq 2.8 \times 10^{-3} \exp - (0.58/kT) \quad (27)$$

was determined in this study from the above data and the Nernst–Einstein relation. It is interesting to note that $D_{V_O^{\cdot\cdot}}$ for SrO-doped CeO_2 is about 20% greater than $D_{V_O^{\cdot\cdot}}$ for CaO-doped CeO_2 at 800°C, whereas at 1000°C both values of $D_{V_O^{\cdot\cdot}}$ are about equal (*20*).

A recent study of oxygen self-diffusion (*19*) in yttria doped ceria at $P_{O_2} = 1$ atm in the temperature range 850–1150°C indicates that the activation energy, approximately 20 kcal/mole, is essentially independent of yttria composition (i.e., for z between 0 and 0.2 in the formula $Ce_{1-2z}Y_{2z}O_{2-z}$). The activation energy obtained in this study (~13 kcal/mole) for diffusion of oxygen vacancies produced by SrO is about 1 kcal less than observed in a similar study (*20*) on CaO-doped CeO_2 and about 7 kcal less than the value reported for self-diffusion of oxygen in $Ce_{1-2z}Y_{2z}O_{2-z}$.

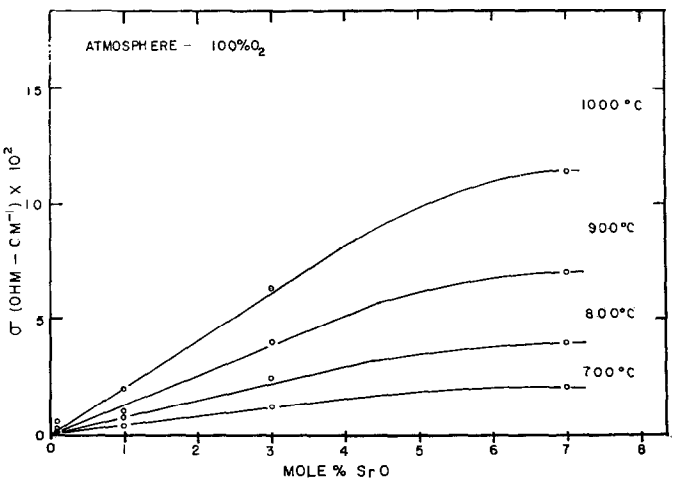

FIG. 12. Isothermal plot of σ versus mole% SrO in CeO_2 at 1 atm O_2.

The calculated dependence of the electronic conductivity on P_{O_2} for the 1 and 3 mole% SrO doped specimens was determined by subtracting σ_i (obtained from Eq. (26)) from the total conductivities shown in Figs. 7 and 8. For the 7 mole% SrO sample, σ_i was assumed equal to the conductivity at high oxygen pressures where σ is independent of P_{O_2}, because Eq. (26) is limited to compositions of SrO content less than about 3 mole%. It should be pointed out that the above procedure for calculating σ_e assumes that σ_i is independent of P_{O_2} (i.e., the concentration of oxygen vacancies is fixed by the dopant concentration, $y > x$). This assumption is true at high oxygen pressures, but at lower oxygen pressures the total oxygen vacancy concentration will be dependent on both y and x and thus will be a function of P_{O_2}. It would be expected that the above assumption is limited to the composition region where $x < 0.1y$. However, it can be shown easily that the error in calculating σ_e using the above procedure in the P_{O_2} region where $x > 0.1y$ is less than 5%, because the electronic mobility is approximately 20 times larger than mobility of the oxygen vacancies (*26*). Typical results of these calculations are shown in Fig. 14 as isothermal plots of log σ_e versus log P_{O_2} for the 1 mole% SrO_2 specimen.

An interesting observation to be made from these plots is that at lower and intermediate temperatures

$$\sigma_e \propto P_{O_2}^{-1/4} \tag{28}$$

over a significant range of oxygen pressures for all of the SrO-doped samples. Increasing the SrO content increases the range of oxygen pressure for which Eq. (28) applies. Since according to Eq. (17),

$$n_{Ce'_{Ce}} \propto x,$$

it can be shown readily that Eq. (28) is consistent with Eq. (23),

$$x \propto P_{O_2}^{-1/4}$$

obtained from the thermodynamic study.

Using the law of mass action and the nonstoichiometric defect reaction represented by Eq. (6), equations can be derived showing the $P_{O_2}^{-1/4}$ dependence of σ_e and x for the case where $y > x$ and $\Delta\bar{H}_{O_2}$ is a constant.

The compositional and temperature dependence of the electronic conductivity of $Ce_{1-y}Sr_yO_{2-y-x}$, $\sigma_e = \sigma_e(x,T)_y$, was determined by drawing smooth curves through the isotherms of log σ_e versus log P_{O_2} and log x versus log P_{O_2} data and selecting values of σ and x that correspond to the same values of y,

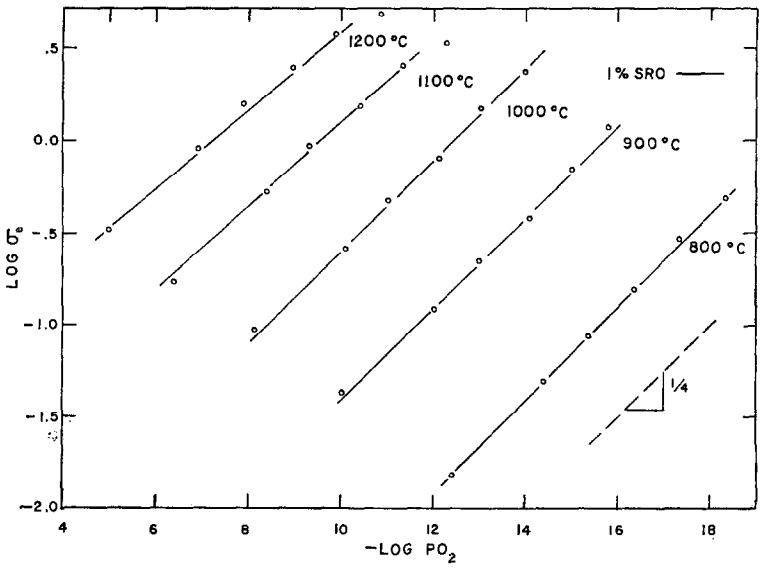

FIG. 14. An isothermal plot of log σ_e versus log P_{O_2} for 1 mole% SrO-doped CeO_2.

P_{O_2}, and T. Typical results of this combined analysis are shown in Fig. 15 where isotherms of log σ_e are plotted as a function of log x for fixed values of y (i.e., $y = 0.01$ and 0.07). For comparative purposes the results of a recent study (*17*) on pure CeO_{2-x} also are shown in Fig. 15.

Although the combined data for the 1 mole% SrO doped sample is available at 25°C increments between 800 and 1050°C and 100°C increments between 1100 and 1500°C, respectively, only data at 800, 1000, and 1200°C are shown in this figure to simplify the presentation of the data. The smallest value of x for each isotherm is determined by the constraint that the error in x be less than 2%. The results for the 7 mole% SrO are shown only for 1000 and 1200°C isotherms because of the limited amount of thermodynamic data available for this composition.

The electronic conductivity of the SrO-doped CeO_2 specimens exhibit essentially the same dependence on x as pure CeO_{2-x} (Eq. (*16*)), except the magnitude of the electronic conductivity decreases with increasing SrO content. Thus, it appears that electronic conductivity of the SrO specimens may be rationalized in terms of the same model as proposed for pure CeO_{2-x}. In the composition region (i.e., x less than approximately 10^{-2}), where $\sigma_e \propto x$, Eq. (22), the concentration of electronic carrier is given by Eq. (17), $n_{Ce'_{Ce}} = 8x/a_o^3$, and the electron mobility appears to be independent of x for a fixed dopant concentration. At larger deviations from stoichiometry, Eq. (17) is assumed to be valid, the nonlinear dependence of σ_e on x however is attributed to the variation of the activation energy (Eq. (21)) for electron transport with x. The electron mobility for pure CeO_{2-x} is given by Eq. (18). If the above interpretation of electronic conduction in SrO-doped CeO_2 is correct then, as shown in Fig. 15, the preexponential term in Eq. (18) decreases with increasing SrO content. As a first-order approximation it would be expected that for $Ce_{1-y}Sr_yO_{2-y-x}$

$$\mu_e \propto (1 - y) \tag{29}$$

when $y > x$. According to Eq. (29), σ_e for the 1 and 7 mole% SrO-doped specimens should decrease 1 and 7%, respectively. As shown in Fig. 15, the observed decrease in σ_e with SrO content is greater than predicted by Eq. (29). To obtain a more quantitative determination of the dependence of μ_e on SrO dopant

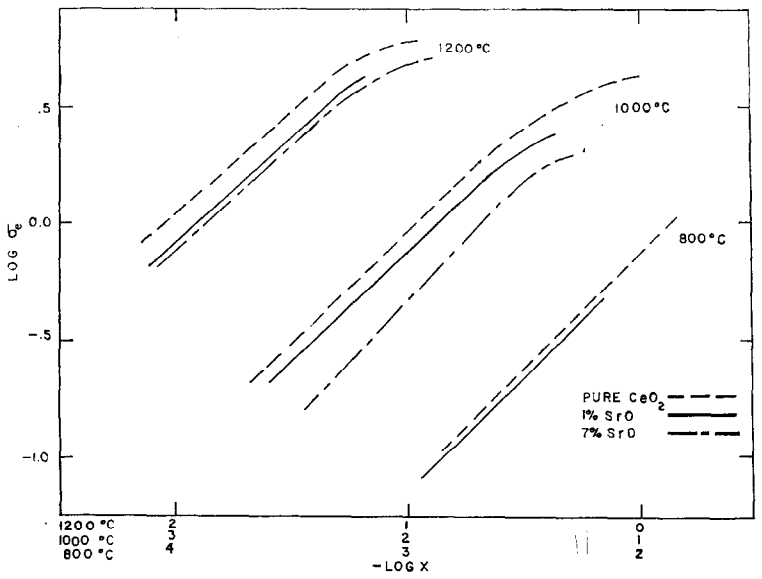

FIG. 15. A comparison of the isothermal plot of log σ_e versus log x, obtained by combining conductivity and thermodynamic data for pure nonstoichiometric CeO_2 and CeO_2 doped with 1 and 7 mole% SrO.

concentration would require additional electrical conductivity and thermodynamic data on samples with several different dopant concentrations.

One other observation to be made from Fig. 15 is the relative temperature dependence of σ_e for pure CeO_{2-x} and the sample doped with 1 mole% SrO. As shown in Fig. 15, σ_e for pure CeO_{2-x} exhibits a slightly greater increase in magnitude with increasing temperature than σ_e for the 1 mole% SrO, which would imply that Q for electron transport (Eqs. (18) and (21) is slightly smaller for the 1% SrO-doped sample. However, because of the aforementioned limitation imposed on the calculation of σ_e, it is difficult to say at this time whether this apparent small decrease in Q with addition of 1 mole% SrO is a real effect.

A study of the transference measurements of SrO-doped CeO_2 to determine t_i as a function of temperature, P_{O_2} and SrO content would provide data that could be combined with the above σ data to determine the dependence of σ_e and σ_i on T, P_{O_2} and SrO content. The combined results of these type of studies would permit an independent test of the simple limiting case defect models for ionic and electronic conductivities proposed in this investigation.

References

1. G. Brauer, K. A. Gingerich, and U. Holtzschmidt, *J. Inorg. Nucl. Chem.* **16**, 77 (1960).
2. G. Brauer and K. A. Gingerich, *J. Inorg. Nucl. Chem.* **16**, 87 (1960).
3. D. J. M. Bevan and J. Kordis, *J. Inorg. Nucl. Chem.* **26**, 1509 (1964).
4. R. J. Panlener, Ph.D. Dissertation, Marquette University, Milwaukee, Wisconsin (1972).
5. R. J. Panlener, R. N. Blumenthal, and J. E. Garnier, *J. Phys. Chem. Solid*, **36**, 1213 (1975).
6. F. A. Kuznetsov, V. I. Beliy, and T. N. Rezukhina, *Doklady Akad. Nauk USSR, Fiz-Khim.* **139**, No. 6, 1405 (1961).
7. H. H. Mobius, *Z. Chem.* **4**, 81 (1964).
8. J. Rudolph, *Z. Naturforsch.* **14**, 727 (1959).
9. E. H. Greener, J. M. Wimmer, and W. M. Hirthe, "Rare Earth Research II" (Karl S. Vorres, Ed.), p. 539, Gordon and Breach, New York (1964).
10. C. J. Kevane, *Phys. Rev.* **133**, A1431 (1964).
11. I. V. Vinokurov, Z. N. Zonn, and V. A. Ioffe, *Sov. Phys.-Solid State* (English transl.) **9**, 2659 (1968).
12. R. N. Blumenthal and J. E. Laubach, "Anisotropy in Single-Crystal Refractory Compounds," Vol. 2, p. 137, Plenum Press, New York (1968).
13. R. N. Blumenthal, P. W. Lee, and R. J. Panlener *J. Electrochem. Soc.* **118**, 123 (1971).
14. R. N. Blumenthal and R. J. Panlener, *J. Phys. Chem. Solids* **31**, 1190 (1970).
15. F. S. Brugner and R. N. Blumenthal, *J. Amer. Ceram. Soc.* **54**, 57 (1971).
16. R. N. Blumenthal and R. L. Hofmaier, *J. Electrochem. Soc.* **121**, 126 (1974).
17. R. N. Blumenthal and R. K. Sharma, *J. Solid State Chem.*, **13**, 360 (1975).
18. J. Faber, Ph.D. Dissertation, Marquette University, Milwaukee, Wisconsin, 1973.
19. B. C. H. Steele and J. M. Floyd, *Proc. Brit. Ceram. Soc.* **19**, 55 (1971).
20. R. N. Blumenthal, F. S. Brugner, and J. E. Garnier, *J. Electrochem. Soc.* **120**, 1230 (1973).
21. J. E. Garnier, R. N. Blumenthal, and R. J. Panlener, submitted for publication.
22. F. A. Kröger, "The Chemistry of Imperfect Crystals," North-Holland, Amsterdam (1964).
23. J. E. Garnier, Ph.D. Dissertation, Marquette University, Milwaukee, Wisconsin (1974).
24. L. S. Darken and R. W. Gurry, *Amer. Chem. Soc.* **67**, 1398 (1945).
25. R. E. Carter and W. L. Roth, *in* "Electromotive Force Measurement in High Temperature Systems" (C. B. Alcock, Ed.), pp. 125–144, American Elsevier, New York (1968).
26. G. J. VanHandel and R. N. Blumenthal, *J. Electrochem. Soc.* **121**, 1198 (1974).